Simulating Optical Pumping in the Laser Spectroscopy Experiment at TRIUMF

Julien Refour

Masters of Science

Department of Physics

McGill University

Montreal,Quebec

2017-09-15

Requirements Statement

DEDICATION

This document is dedicated to the graduate students of the McGill University.

ACKNOWLEDGEMENTS

Acknowledgments, if included, must be written in complete sentences. Do not use direct address. For example, instead of Thanks, Mom and Dad!, you should say I thank my parents.

ABSTRACT

Abstract in English and French are required. The text of the abstract in English begins here.

ABRÉGÉ

The text of the abstract in French begins here.

TABLE OF CONTENTS

LIST OF TABLES

Table page

LIST OF FIGURES

CHAPTER 1
Introduction

CHAPTER 2
Laser Spectroscopy at TRIUMF

This chapter is intended as a brief introduction to the laser spectroscopy experiment present at TRIUMF, with special emphasis on the parts relevant to this work. A more complete description of the experiment can be found in [1].

Located in the ISAC I (Isotope Separator and ACcelerator) experimental hall at TRIUMF, as shown in Fig. 2–1, the Laser Spectroscopy experiment at TRIUMF, more specifically known as the Collinear Fast-Beam laser Spectroscopy (CFBS) experiment, is shown in Fig. 2–2.

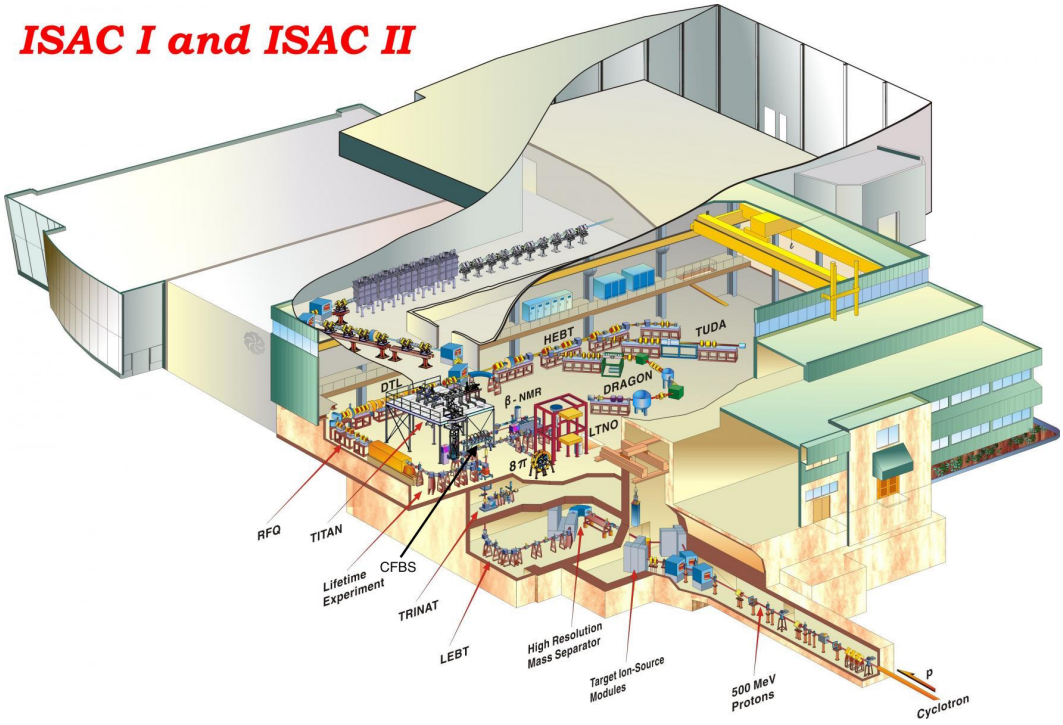

Figure 2–1: The location of the CFBS experiment within the ISAC I experimental hall, as well as the locations of the beamline and other experiments present at TRIUMF.

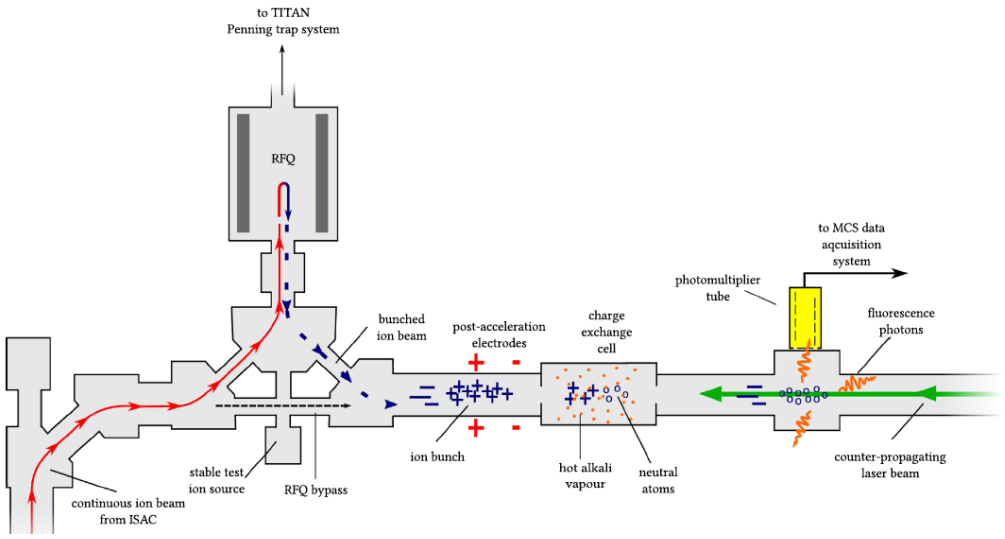

Figure 2–2: Schematic of the CFBS experiment at TRIUMF.[1] Radioactive ions produced in the target area are accelerated towards the experiment, entering just before the RFQ trap, where they can be bunched or allowed to continue unimpeded. The ions then pass through the CEC, where they collide with an alkali vapour. In the region between the CEC and the LCR, the atoms interact with a counter-propagating laser. This region is a blind spot where emitted photons cannot be measured and is the main focus of this work.

At TRIUMF, radioactive atoms are produced through the collision of protons, accelerated by the 500 MeV cyclotron present on-site, and a target material. The products of the collision are then ionized, accelerated and mass separated using a mass separator with resolution $m/\Delta m \approx 5000$, where m is the mass of the atom. [1] After the required atoms have been selected, they are then directed to the CFBS experiment, detailed below.

2.1 Radio Frequency Quadrupole (RFQ) Trap

The ions enter the CFBS experiment as a continuous beam, where they first encounter a radio frequency quadrupole (RFQ) Paul Trap [1]. Here, the atoms can enter the RFQ trap and collect for a pre-determined collection time, after which they are released in bunches. Bunching the atoms is done to reduce background counts. Briefly, the light collection system is triggered on the release of the ion bunches, reducing the available time for background photons

to be counted. As the light collection system is only sensitive to photons for the time window during which the ion bunch passes through the interaction region, background counts are also only collected for this time. Alternatively, photons are collected continuously, whether or not there are resonant ions in the interaction region, allowing the signal to background ration to diminish over time.

2.2 Charge Exchange Cell (CEC)

If the aim is to investigate transitions in a neutral atom, then the ions must regain their lost electron. This is the role of the charge exchange cell (CEC), shown in detail in Fig. 2–3. Using an alkali-metal vapour that is circulated perpendicularly to the direction of the beam, the CEC provides a source of electrons for the oncoming ions to capture. This introduces an issue, however. As the alkali-metal vapour can not be entirely contained to the CEC, any light collection instruments, such as a photo-multiplier tube, must be located further down the beamline. This is done to avoid the growth of an alkali-metal coating on the light-collection surfaces, which would significantly hamper the collection of resonant photons as the experiment progresses. This decision provides the *raison d'être* for this work, as it introduces the opportunity for optical pumping, discussed in detail in Chapter 4. Since the ions are neutralized in the CEC, they can no longer be accelerated through the use of an electrostatic potential. As such, they must be brought into resonance before they enter the interaction region. This is done using a set of electrodes present in front of the CEC, shown in Fig. 2–2.

In the case of transitions present in the ion, then the CEC is unneeded, and the final acceleration is done using a mesh present within the LCR, detailed in the next section. The location of the mesh is chosen such that the ions are in resonance just as they pass the light collection system, removing the

possibility that optical pumping could significantly affect the results of the experiment.

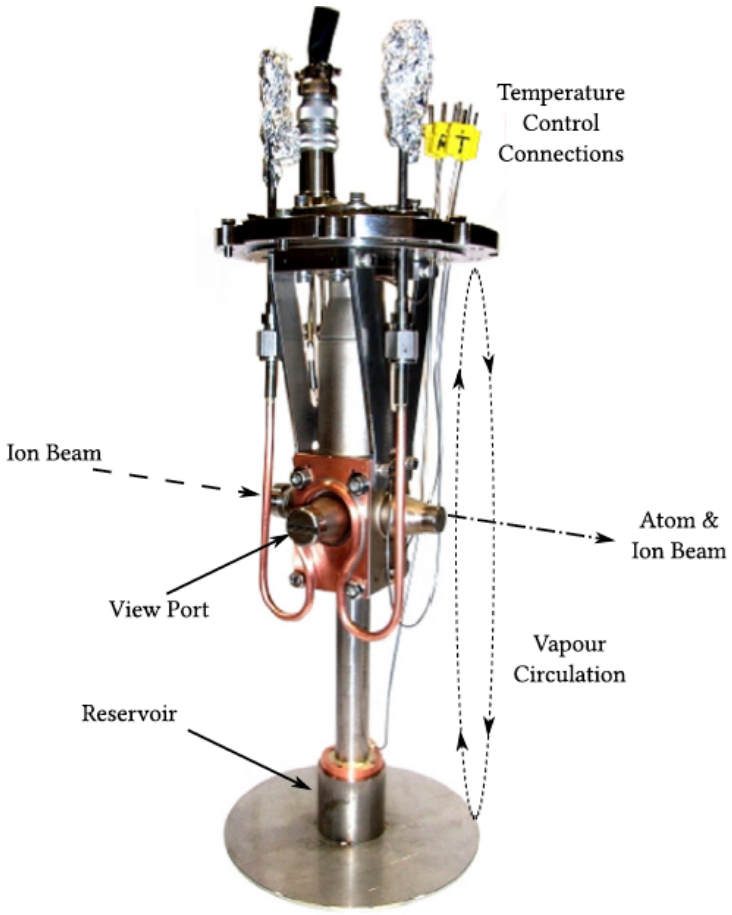

Figure 2–3: The charge exchange cell allows oncoming ions to be neutralized through collision with a perpendicularly flowing alkali-metal vapour.[1]

2.3 Light Collection Region (LCR)

Located roughly 40 cm down the beamline from the CEC, the light collection region (LCR) (Fig. 2–4) houses the equipment necessary for detecting the photons emitted when a beam of ions/atoms is in resonance with a counter propagating laser. A concave mirror located opposite the photo-multiplier tube (PMT) allows all photons within the 5% solid angle of the detection system to be collected by a series of light collection optics, placed in front of the

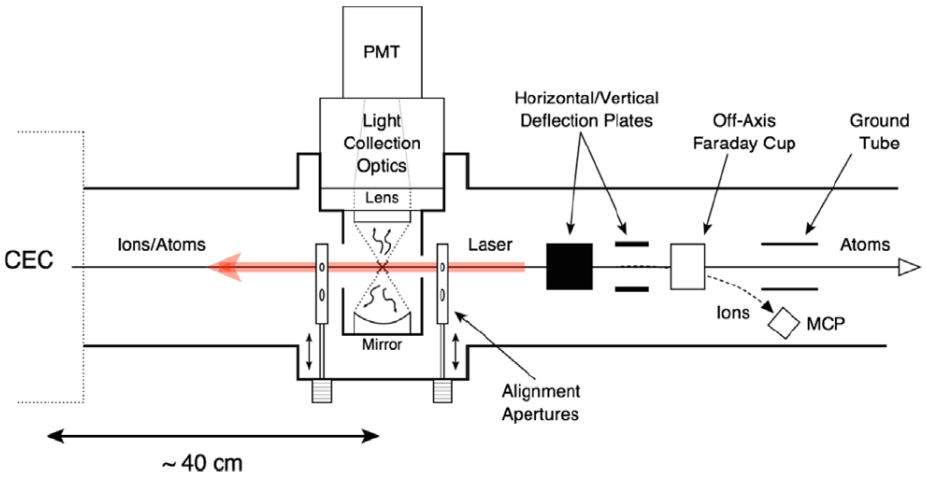

Figure 2–4: Schematic of the light collection region. Photons emitted through atom/laser interactions are directed towards a photo-multiplier tube using a combination of mirrors and lenses. [1]

PMT, designed to optimize photon detection efficiency at a particular wavelength. Using knowledge of the laser frequency, the beam energy and photon counts, the energies of the hyperfine transitions can be determined.

CHAPTER 3
Theory of Laser Spectroscopy

In this chapter, the theoretical background necessary to the understanding and simulation of a hyperfine spectrum is presented. In § 3.1, the features of a hyperfine spectrum are liked to physical properties a nucleus. Next, § 3.2 outlines the way in which lasers interact with atoms Note: Throughout this section, a variable written in a bold typeface is vector valued, while its non-bold counterpart is its magnitude.

3.1 Anatomy of A Hyperfine Spectrum

How can the properties of a hyperfine spectrum, such as that of ^{69}Ga shown in Fig. 3–1, be translated into measurements of the physical properties of the nucleus? The hyperfine spectrum is, after all, the result of probing the electronic structure of the atom. The answer, of course, is that the electrons interact with the nucleus through several mechanisms, each of which will be described in this section. To begin, however, consider the following system: An electron transitions from a ground state $|g\rangle$ to an excited state $|e\rangle$. More precisely $|g\rangle$ and $|e\rangle$ are defined as

$$|g\rangle = |n_g, \mathrm{L_g}, \mathrm{L_{g,z}}\rangle \tag{3.1}$$

$$|e\rangle = |n_e, \mathrm{L_e}, \mathrm{L_{e,z}}\rangle \tag{3.2}$$

where $n_{g,e}$ are principal quantum numbers, $\mathbf{L_{g,e}}$ the orbital angular momenta, and $\mathrm{L}^z_{g,e}$ the projections of the orbital angular momentum on an axis of quantization z. Next, if nucleus of the atom in which this transition is occurring has angular momentum $\mathbf{I}$, then a quantity, $\mathbf{F}$, can be defined as

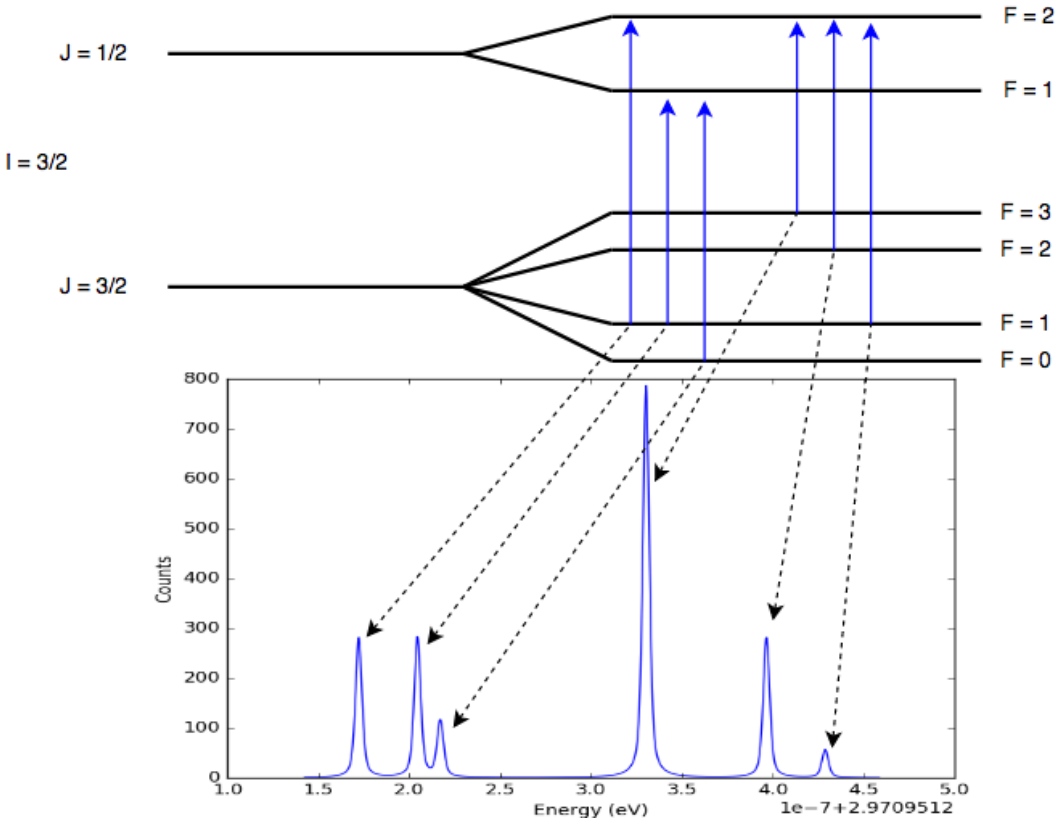

Figure 3–1: Hyperfine spectrum of Gallium-69 for the $4P_{3/2} \rightarrow 5S_{1/2}$ transition. Photon counts are shown on the vertical axis, while the horizontal axis gives relative frequency with respect to the fine transition. The errorbars are standard Poisson counting errors.

$$\mathbf{F_{g,e}} = \mathbf{I} + \mathbf{L_{g,e}} \tag{3.3}$$

$\mathbf{F}$ describes the total angular momentum state of the atom, so $|g\rangle$ and $|e\rangle$ can be rewritten as

$$|g\rangle = |n_g, \mathrm{F_g}, \mathrm{F_{g,z}}\rangle \tag{3.4}$$

$$|e\rangle = |n_e, \mathrm{F_e}, \mathrm{F_{e,z}}\rangle \tag{3.5}$$

For a fixed $\mathbf{I}$, $\mathbf{F}$ can range from $(-\mathrm{L} + \mathrm{I})$ to $(\mathrm{L} + \mathrm{I})$.

3.1.1 Peak Energies

The energy of the electrons depends on the various electron-nucleus interactions present in the atom. If for the purposes of this work, only three interactions produce measurable changes in the energies of the electron levels. These are the isotope, magnetic dipole and electric quadrupole shifts, which lead to energy shifts on the order of roughly $10^{-7} - 10^{-4}$ eV [3]. There are higher order interactions (magnetic octopole, electric hexadecapole), however their effects are far below the resolution of $\approx 10^{-8}$ eV of the experimental set-up employed at TRIUMF.[6]

Isotope Shift

The isotope shift is measured with respect to a reference isotope. As neutrons are added or removed from a nucleus, the charge distribution, as well as the mass, of the nucleus changes. This leads to three different effects on the energies of the electrons.

The change in the mass of the nucleus leads to what is known as the Mass shift, ΔE_M. The mass shift between two isotopes with mass numbers A and A' is given by

$$\Delta E_M = \frac{m_{\mathrm{A}} - m_{\mathrm{A}'}}{2 m_{\mathrm{A}} m_{\mathrm{A}'}} \left(\sum_i \mathbf{p}_i + 2 \sum_{i>j} \mathbf{p}_i \cdot \mathbf{p}_j \right) \tag{3.6}$$

where m_{A} and $m_{\mathrm{A}'}$ are the isotope masses, and the $\mathbf{p}_i$ are the electron momenta. The first term is due to the nucleus recoiling with the electrons when a photon is absorbed, while the second term deals with the electron-electron interactions.

The change in the charge distribution of the nucleus produces the Field shift. While the typical nucleus is far smaller the wavefunction of a typical orbital electron, the effect is still important. The energy of a nucleus in the charge density produced by the electrons at the origin, E_F, is given by

$$E_F = \frac{Ze^2}{6\epsilon_0}|\psi(0)|^2 \left\langle r_{ch}^2 \right\rangle \tag{3.7}$$

where ϵ_0 is the permitivity of free space, Z is the proton number, e is the fundamental charge and $\langle r_{ch}^2 \rangle$ is the mean-square charge radius of the nucleus, defined as

$$\left\langle r_{ch}^2 \right\rangle = \frac{\int_0^\infty \rho(\mathbf{r}) r^2 dV}{\int_0^\infty \rho(\mathbf{r}) dV} \tag{3.8}$$

The field shift between two isotopes is then given by

$$\Delta E_F = \frac{Ze^2}{6\epsilon_0}\Delta|\psi(0)|^2 \Delta \left\langle r_{ch}^2 \right\rangle \tag{3.9}$$

In total, then, the isotope shift $\Delta E_{\mathrm{A,A'}}$ is given by

$$\Delta E_{\mathrm{A,A'}} = \Delta E_M + \Delta E_F \tag{3.10}$$

Magnetic Dipole Shift

A nucleus with a non-zero nuclear spin $\mathbf{I}$ will have a magnetic dipole moment, given by

$$\boldsymbol{\mu}_\mathbf{I} = g_\mathrm{I}\mu_\mathrm{N}\mathbf{I} \tag{3.11}$$

where g_I is the g-factor and μ_N is the nuclear magneton.[2] The interaction of μ_I with the magnetic field produced by the electrons, $\mathbf{B_e}$, creates a shift in the energy of the orbiting electrons. Provided the electrons occupy an angular momentum state $\mathbf{L} \neq 0$, the hamiltonian for this interaction is given by

$$\mathcal{H} = -\boldsymbol{\mu}_\mathbf{I} \cdot \mathbf{B_e} \tag{3.12}$$

This interaction leads to a shift, ΔE_{μ_I}, in the energy of the atomic states by

$$\Delta E_{\mu_I} = \frac{AK}{2} \tag{3.13}$$

where $K = \mathrm{F(F+1) - I(I+1) - L(L+1)}$ and

$$A = \frac{\mu_\mathrm{I} \mathrm{B_e}}{\mathrm{IL}} \tag{3.14}$$

Electric Quadrupole Shift

The electric quadrupole moment is used to describe the distribution of charge in a nucleus. For a nucleus composed of n protons and $\mathbf{I} \geq 1$, the electric quadrupole moment, Q, is given by

$$\mathrm{Q} = \sum_i^n (3z_i^2 - r_i^2) \tag{3.15}$$

where $r_i^2 = x_i^2 + y_i^2 + z_i^2$. Noting that the deformations described by Q are defined with respect to the $z-$axis, Fig. 3.1.1 shows how different values of Q translate into physical differences in the charge distribution of the nucleus. If $\mathrm{Q} < 0$, then the nucleus is stretched in the $x - y$ plane (oblate). If $\mathrm{Q} > 0$, then the nucleus is stretched along the $z-$axis (prolate). $\mathrm{Q} = 0$ indicates that the nucleus is spherical.

In reality, direct measurement of Q is not feasible, as the nucleus is rotating. Instead, the spectroscopic quadrupole, Q_s, is measured. Q_s is defined as the projection of Q onto the axis of quantization of the nucleus, and is given by

$$\mathrm{Q}_s = \frac{\mathrm{I(2I-1)}}{\mathrm{(I+1)(2I+3)}} \mathrm{Q} \tag{3.16}$$

The use of Q_s as a measure of Q is valid under the assumption that the nuclear deformation is axially symmetric. Additionally, it is assumed that the axis of symmetry has a well defined direction with respect to $\mathbf{I}$.

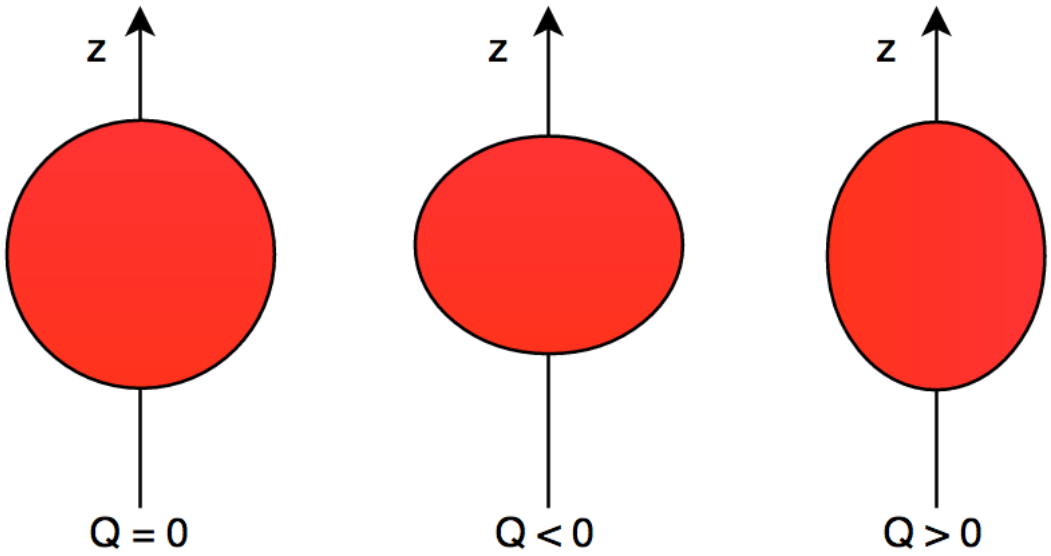

Figure 3–2: Shape of the nucleus for Q = 0 (spherical), Q < 0 (oblate) and Q > 0 (prolate).

The hamiltonian for the interaction between the spectroscopic electric quadrupole moment and the electric field produced by the electrons at the nucleus, E_N, is given by

$$\mathcal{H} = -\frac{1}{6} e\mathrm{Q}_s \nabla E_N \tag{3.17}$$

where

$$\nabla E_N = \frac{\partial^2 V}{\partial x_i \partial x_j}, \{x_j, x_k\} \in \{x, y, z\} \otimes \{x, y, z\} \tag{3.18}$$

e is the fundamental charge and V is the electric potential. Recalling that the nuclear deformation is symmetric about the axis of quantization, the shift in energy is then given by

$$\Delta E_{\mathrm{Q_s}} = \frac{B}{4} \left[\frac{\frac{3}{2} K(K+1) - 2\mathrm{I}(\mathrm{I}+1)\mathrm{L}(\mathrm{L}+1)}{\mathrm{I}(2\mathrm{I}-1)\mathrm{L}(2\mathrm{L}-1)} \right] \tag{3.19}$$

where B is a hyperfine coefficient and is given by

$$B = e\mathrm{Q_s} \left\langle \frac{\partial^2 V}{\partial z^2} \right\rangle \tag{3.20}$$

Eq. 3.19 has singularities at $\mathbf{I} = \frac{1}{2}$ and $\mathbf{L}=\frac{1}{2}$. This captures the fact that in either case there is no coupling between the nucleus and the electrons, as an orbital angular momentum state of $\frac{1}{2}$ is isotropically distributed in space .

The Hyperfine Equation

The resonant energy of a transition between $|g\rangle = |n_g, \mathbf{F}_\mathrm{g} = \mathbf{I} + \mathbf{L}_\mathrm{g}\rangle$ and $|e\rangle = |n_e, \mathbf{F}_\mathrm{e} = \mathbf{I} + \mathbf{L}_\mathrm{e}\rangle$ is then given by

$$E_{hfs} = E_{fs} + \Delta E_{\mathrm{A,A'}} + \Delta E_{\mu_I}\Big|_{\mathrm{F_g},I,L_g}^{\mathrm{F_e},I,L_e} + \Delta E_{\mathrm{Q_s}}\Big|_{\mathrm{F_g},I,L_g}^{\mathrm{F_e},I,L_e} \tag{3.21}$$

When a hyperfine spectrum is fit, the fit parameters which govern the locations of the peaks are the hyperfine parameters A and B for both $|e\rangle$ and $|g\rangle$, as well as what is known as the centroid, ν_0. The centroid combines the fine structure energy and the isotope shift into one quantity. It is important to note that while the values of hyperfine coefficients can be directly linked to the physical properties of the nucleus, only the change in the centroid with respect to a reference isotope can be used to measure the change in the mean-square charge radius.

3.1.2 Peak intensities

The other notable characteristic of a hyperfine spectrum, the ratios of the peak intensities can give information as to the spin of the nucleus if the angular momentum states of the electron orbitals are known. In the Angular Part of § 3.2, the origin of the peak intensities is presented in more detail. In the interest of the completeness of this section, the result is presented here. The relative intensity of a transition from $|\mathrm{F_e}, \mathrm{J_e}, \mathrm{I}\rangle$ to $|\mathrm{F_g}, \mathrm{J_g}, \mathrm{I}\rangle$, known as the Racah intensity, is

$$Intensity = (2F_e + 1)(2F_g + 1) \begin{Bmatrix} F_g & F_e & 1 \\ J_e & J_g & I \end{Bmatrix}^2 \tag{3.22}$$

where the quantity in curly brackets is the Wigner 6-j symbol. (CITE TOM)

3.1.3 Peak Widths

The lineshape of the peaks is the result of three physical processes, outlined in this section. These three processes are of varying importance, depending on the properties of the atoms being probed, contributing Lorentzian or Gaussian profiles to the peak shape.

Natural Linewidth

The first cause of broadening is the natural linewidth of an atomic transition. The energy-time version of the uncertainty principal, $\Delta E \Delta t = \hbar$ leads to

$$\Delta\nu = \frac{\Delta E}{h} = \frac{1}{2\pi\tau_0} \tag{3.23}$$

where τ_0 is the mean lifetime of the state and $\Delta\nu$ is the full width half maximum of the Lorentzian profile describing the natural lineshape of an atomic transition.[5]

Power Broadening

Stimulated emission occurs when an atom in an excited state is in the presence of photons with energy similar to an available atomic transition. In the case of laser spectroscopy, the laser provides the source of stimulating photons. Stimulated emission leads to power broadening, which depends on the power of the laser. The lifetime of a state will decrease according to

$$\frac{1}{\tau} = \frac{1}{\tau_0}\sqrt{1 + \frac{I}{I_s}} \tag{3.24}$$

where I is the laser intensity and I_s is the saturating laser intensity, which occurs when the rate of absorbtion is equal to the rate of stimulated emission on resonance. Power broadening leads to a Lorentzian lineshape.[5]

Doppler Broadening

Doppler broadening occurs when the atoms have a thermal velocity spread along the direction of propagation. This velocity spread leads to a relativistic shift in the frequency of the laser observed by the atoms. The shift in frequency, $\delta\nu$, is given by

$$\delta\nu = \nu_0 \left(\frac{8kT\log(2)}{m_A c^2} \right)^{1/2} \tag{3.25}$$

where T is the absolute temperature of the atoms in Kelvin, k is the Boltzmann constant and m_A is the atomic mass. Doppler broadening contributes a Gaussian broadening to the lineshape of the transition.[5]

Voigt Profile

As the strengths of the above processes can change depending on the parameters of the experiment, a Voigt profile is used when fitting the hyperfine spectra. The Voigt profile is a convolution of the Lorentzian and Gaussian profiles, and is thus difficult to evaluate in an algorithmic manner. For the purposes of this work, the Pseudo-Voigt profile, given below, is used.

$$\mathcal{V}(x) = \frac{1-\epsilon}{\sigma_g\sqrt{2\pi}} \exp\left(\frac{(x-x_0)^2}{2\sigma_g^2} \right) + \frac{\epsilon\sigma}{\pi((x-x_0)^2+\sigma^2)} \tag{3.26}$$

where ϵ is a parameter that determines the relative contribution of the Gaussian and Lorentzian profiles and x_0 is the centroid. σ is the Voigt linewidth and $\sigma_g = \sigma/\sqrt{2\log 2}$ is defined such that the full width half maximum of the profile as well as it's components is 2σ.[4]

3.2 Spontaneous Emission in Multi-Level Atoms

A hyperfine spectrum is constructed through the measurement of the photons emitted as electrons in excited states de-excite to lower energy states. In order to simulate a hyperfine spectrum, then, it is necessary to understand

the mechanisms through which electrons transition between energy levels in an atom.

Consider a two-level atom in an excited state. After a time t, the atom transitions to the ground state. The wavefunction of the system is given by

$$|\psi\rangle = c_{e,0}e^{-i\omega_e t}\,|e,0\rangle + \sum_S c_{g,1}e^{-i(\omega_g+\omega)t}\,|g,1_S\rangle \tag{3.27}$$

where $S = (\boldsymbol{k}, \boldsymbol{\varepsilon})$ gives the wavevector $\boldsymbol{k}$ and polarization $\boldsymbol{\varepsilon}$ of an emitted photon, $\omega = kc$, ω_e and ω_g are the energies of the excited and ground states, respectively (REFERENCE NEEDED). The time evolution of the two states is described by

$$i\frac{\mathrm{d}c_{e,0}(t)}{\mathrm{d}t} = \sum_S c_{g,1_S}(t)\Omega_S e^{-i(\omega-\omega_a)t} \tag{3.28}$$

$$i\frac{\mathrm{d}c_{g,1_S}(t)}{\mathrm{d}t} = c_{e,0}(t)\Omega_S^* e^{i(\omega-\omega_a)t} \tag{3.29}$$

where the coupling between each state is given by the Rabi frequency $\Omega_s = -\boldsymbol{\mu}\cdot\boldsymbol{E}_\omega/\hbar$. The electric dipole moment, $\boldsymbol{\mu}$ between two states is given by

$$\boldsymbol{\mu} = e\,\langle e|\,\boldsymbol{r}\,|g\rangle \tag{3.30}$$

and the electric field per mode is given by

$$\boldsymbol{E}_\omega = \sqrt{\frac{\hbar\omega}{2\epsilon_0 V}}\boldsymbol{\varepsilon} \tag{3.31}$$

V is the volume over which the field is quantized and will eventually drop out. Integration of Eq.1.24 and substitution of the result into Eq.1.23, followed by further integration yields

$$\frac{dc_{e,0}(t)}{dt} = -\frac{\gamma}{2}c_{e,0}(t) \tag{3.32}$$

where

$$\gamma = \frac{\omega^3 \mu^2}{3\pi\epsilon_0 \hbar c^3} \tag{3.33}$$

is the decay rate for the population of the excited state. ω is the frequency of the transition and c is the speed of light in a vacuum. The mean lifetime of the excited state is given by $\tau = 1/\gamma$. For an excited state where multiple decay paths are available, the total decay rate, γ_t is given by

$$\frac{1}{\gamma_t} = \sum_i \frac{1}{\gamma_i} \tag{3.34}$$

where the γ_i are the partial decay rates for each decay path.

3.2.1 The Dipole Moment

In general, calculating the dipole moment $\mu = \langle e | \boldsymbol{\varepsilon} \cdot \boldsymbol{r} | g \rangle$ is not a simple task. In the simplest case (read hydrogenic wavefunctions), the Wigner-Eckart theorem states that the dipole moment can be split into two separate quantities in the following manner

$$\mu_{eg} = e\mathcal{R}_{n_e L_e, n_g L_g} \mathcal{A}_{L_e L_e^z, L_g L_g^z} \tag{3.35}$$

where $\mathcal{R}_{n_e L_e, n_g L_g}$ and $\mathcal{A}_{L_e L_e^z, L_g L_g^z}$ are the radial and angular parts of the dipole moment, respectively. While both quantities are presented in more depth for the sake of completion (not the word I want to use...), it will become apparent that the hyperfine inter

Radial Part

In most cases where the hyperfine structure is being probed, the radial part of the dipole moment only acts as an overall multiplicative factor for the strength of the coupling between the excited and ground states. This is due to the fact that all available ground states typically share the same radial wavefunction, likewise in the case of the excited states. The radial part is

given by

$$\mathcal{R}_{n_eL_e,n_gL_g} = \langle R_{n_eL_e} | \boldsymbol{r} | R_{n_gL_g} \rangle = \int_0^\infty r^2 R_{n_eL_e}(r) r R_{n_gL_g}(r) dr \tag{3.36}$$

where the R_{nL} are the hydrogenic radial wavefunctions of their respective states

$$R_{nL}(r) = N_{nL}\rho^L \exp(-\rho/2) L_{n-L-1}^{2L+1}(\rho) \tag{3.37}$$

where N_{nL} is a normalization constant and $L_{n-L-1}^{2L+1}(\rho)$ are the Laguerre polynomials evaluated at $\rho = 2r/na_0$, where a_0 is the Bohr radius. The $L_{n-L-1}^{2L+1}(\rho)$ can be expanded in a power series

$$L_n^m(r) = \sum_{k=0}^{n} c_k r^k \tag{3.38}$$

It is possible to extend this analysis to atomic structures that have an isolated electron sitting on top of a closed shell. This is done using the effective principal quantum number $n^* = n - \delta_L$, where δ_L is called the quantum defect and depends on the orbital angular momentum $\mathbf{L}$. This extended analysis is, however, not necessary, as an empirical measure of $\mathcal{R}^2_{n_eL_e,n_gL_g}$ is easily obtained, and remains constant over all hyperfine transitions. This is done through the use of the decay rate of the fine-structure transition, γ_f. As per Eq. 3.34, the decay rate of the fine-structure excited state is given by

$$\frac{1}{\gamma_f} = 3\pi\epsilon_0\hbar c^3 \sum_i \frac{1}{\omega_i^3 \mu_i^2} \tag{3.39}$$

Substitution of Eq. 3.35 in to the above yields

$$\frac{1}{\gamma_f} = \frac{3\pi\epsilon_0\hbar c^3}{\mathcal{R}^2 e^2} \sum_i \frac{1}{\omega_i^3 \mathcal{A}_i^2} \tag{3.40}$$

where the subscripts on $\mathcal{R}$ and $\mathcal{A}$ have been dropped for convenience. Rearranging gives the following expression for $\mathcal{R}^2$

$$\mathcal{R}^2 = \frac{3\pi\epsilon_0\hbar c^3\gamma_f}{e^2}\sum_i \frac{1}{\omega_i^3\mathcal{A}_i^2} \tag{3.41}$$

Note that this result allows $\mathcal{R}$ to take both negative and positive values. For the purposes of the calculations present in this work, however, only the square of the radial part is important. As such, the degeneracy in Eq. 3.41 can safely be ignored.

Angular Part

Unlike the radial part of the dipole moment, the angular part changes depending on the F state of the excited and ground states. An outline of the procedure followed to find $\mathcal{A}$ is outlined in this section, but for a complete treatment of the calculation can be found in (REFERENCE NEEDED)

In the presence of hyperfine structure, the atomic eigenstates can be represented in the following manner

$$|n, F, F_z\rangle = \sum_i C_i \,|n, J, J_z\rangle \,|I, I_z\rangle \tag{3.42}$$

where $\mathbf{J} = \mathbf{L} + \mathbf{S}$, $\mathbf{S}$ is the spin of the electron and the C_i's are Clebsch-Gordan coefficients. The $\mathbf{J}$ states can further be decomposed into combinations of $\mathbf{L}$ and $\mathbf{S}$ states

$$|n, F, F_z\rangle = \sum_i C_i \,|I, I_z\rangle \sum_k C_k \,|n, L, L_z\rangle \,|S, S_z\rangle \tag{3.43}$$

This is possible since the optical electric field only couples the orbital angular momentum, $\mathbf{L}$, components of the eigenstates. The Clebsch-Gordan coefficients can be expressed as

$$C_i = \langle \mathrm{L}, \mathrm{L_z}; \mathrm{S}, \mathrm{S_z}|\mathrm{J}, \mathrm{J_z}\rangle = (-1)^{-\mathrm{L}+\mathrm{S}-\mathrm{J_z}}\sqrt{2\mathrm{J}+1}\begin{pmatrix} \mathrm{L} & \mathrm{S} & \mathrm{J} \\ \mathrm{L}_z & \mathrm{S}_z & -\mathrm{J}_z \end{pmatrix} \tag{3.44}$$

where the quantity in brackets is the Wigner 3-j symbol. Substituting Eq. 3.43 into the definition of μ gives

$$\begin{aligned}\mu = & \sum_{q=-1,0,1} e(-1)^{1+\mathrm{L_e}+\mathrm{S}+\mathrm{J_g}+\mathrm{J_s}+1-\mathrm{F_{e,z}}}\mathcal{R}_{n_eL_e,n_gL_g} \\ & \times\sqrt{(2J_g+1)(2J_e+1)(2F_g+1)(2F_e+1)} \\ & \times\begin{Bmatrix} \mathrm{L}_e & \mathrm{J}_e & \mathrm{S} \\ \mathrm{J}_g & \mathrm{L}_g & 1 \end{Bmatrix}\begin{Bmatrix} \mathrm{J}_e & \mathrm{F}_e & \mathrm{I} \\ \mathrm{F} & \mathrm{J}_g & 1 \end{Bmatrix}\begin{pmatrix} \mathrm{F}_g & 1 & \mathrm{F}_e \\ \mathrm{F}_{g,z} & q & -\mathrm{F}_{e,z} \end{pmatrix}\end{aligned} \tag{3.45}$$

where the quantity in the curly brackets is not a 3-j symbol but a 6-j symbol, and q is the polarization of the electric field (1,0,-1). Recalling that $\mathcal{R}_{n_eL_e,n_gL_g}$ is a multiplying factor only and can be pulled out of the summation, then the angular part of μ is given by

$$\begin{aligned}\mathcal{A} = \sum_{q=-1,0,1} e(-1)^{1+\mathrm{L_e}+\mathrm{S}+\mathrm{J_g}+\mathrm{J_s}+1-\mathrm{F_{e,z}}} & \times\sqrt{(2J_g+1)(2J_e+1)(2F_g+1)(2F_e+1)} \\ & \times\begin{Bmatrix} \mathrm{L}_e & \mathrm{J}_e & \mathrm{S} \\ \mathrm{J}_g & \mathrm{L}_g & 1 \end{Bmatrix}\begin{Bmatrix} \mathrm{J}_e & \mathrm{F}_e & \mathrm{I} \\ \mathrm{F} & \mathrm{J}_g & 1 \end{Bmatrix}\begin{pmatrix} \mathrm{F}_g & 1 & \mathrm{F}_e \\ \mathrm{F}_{g,z} & q & -\mathrm{F}_{e,z} \end{pmatrix}\end{aligned} \tag{3.46}$$

3.2.2 Selection Rules

The coupling of the ground state and excited state through the optical electrical field places restrictions on the change in the angular momentum state of the atom. In the case of transitions between orbital angular momentum states present in hyperfine atomic structures, only transitions where $\Delta\mathbf{F} = \pm 1, 0$ are permitted. These selection rules reflect conservation of angular momentum. Photons have angular momentum $\hbar$. The angular momentum of the photon can either be parallel, anti-parallel or perpendicular to the axis of quantization, reflecting $\Delta\mathbf{F}= \pm 1, 0$ respectively. Additionally, the transition $\mathbf{F}' = 0 \rightarrow \mathbf{F} = 0$ is forbidden. This is because $\mathbf{F}$ is a result of the coupling

between **I** and **L**. **F**' = 0 implies that both **I** = 0 = **L**. The emission of a photon requires a change in angular momentum, which is impossible if **F** = 0.

3.3 Photon Scattering Rates

The rate at which photons are absorbed by atoms is an important factor in the simulation of hyperfine spectra. For a two level system, where the population of the the excited state ρ_e and the ground state ρ_g obey the conservation rule $\rho_e + \rho_g = 1$, the total scattering rate from a laser field is given by,

$$\gamma_p = \frac{s_0/2}{1 + s_0 + (2\delta/\gamma)^2} \tag{3.47}$$

where s_0 is the on resonance saturation parameter $s_0 = I_l/I_s$, δ is the detuning parameter and γ is the decay rate of the excited state. I_l is the intensity of the laser field and I_s is the saturation intensity defined as

$$I_s \equiv \frac{\pi hc}{3\lambda^3\tau} \tag{3.48}$$

where λ is the wavelength of emission of a resonant photon and $\tau = 1/\gamma$ is the lifetime of the excited state. The detuning parameter can be defined as

$$\delta = |f_l - f_{res}| \tag{3.49}$$

where f_l is the frequency of the laser and f_{res} is the resonant frequency of the transition.

CHAPTER 4
Simulation of Optical Pumping

As mentioned in the previous chapter, the distance between the CEC and the LCR introduces the possibility of optical pumping, a process that changes the ground state distribution of the atoms as they travel the distance between the two regions. This change in ground state distribution is induced by the interaction of the atoms with the laser before they reach the LCR. In an atomic system that has not interacted with a laser, the ground state distribution of the hyperfine levels is statistical (REFERENCE). The likelihood of an electron occupying hyperfine level **F** is proportional to $2F + 1$. In a system with N hyperfine ground states, each with $\mathbf{F} = \mathbf{F}_n$, where n = 1,2,3,..N, the probability of an electron occupying, say, the i-th level is given by (REFERENCE NEEDED)

$$\mathrm{Prob(F}_i) = \frac{2F_i + 1}{\sum_{j=1}^{\mathrm{N}} 2F_j + 1} \tag{4.1}$$

However, as the electron goes through a series of excitation/decay cycles, certain ground states will be selected over others, depending on selection rules as well as transition probabilities. Optical pumping manifests itself through the modification of the relative peak heights in a hyperfine spectrum, as shown in Fig. 4–1, where the peak heights of a hyperfine spectrum of francium show the effects of optical pumping. The expected peak heights as calculated by, i.e. the Racah intensities are shown in red, and are compared to the intensities measured with the laser continuously on (solid black) and those measured when the laser was pulsed (black outline). The pulsed intensities are similar

to the expected intensities, while those measured with a continuous wave (cw) laser deviate significantly.

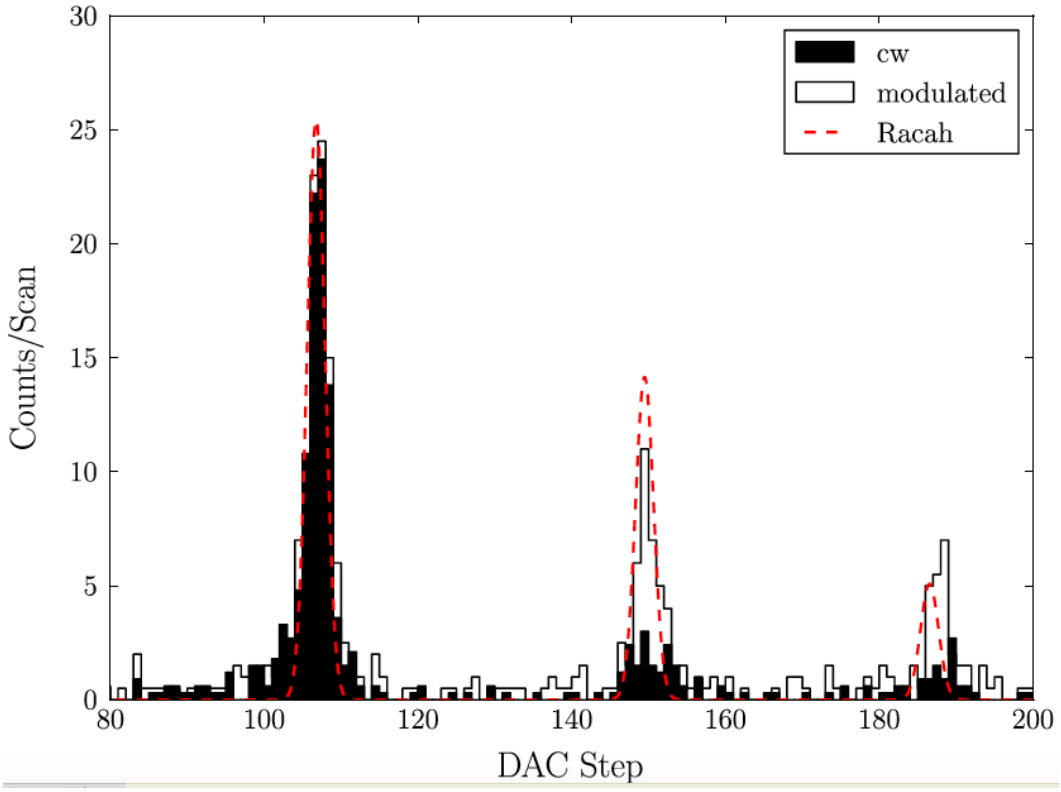

Figure 4–1: Demonstration of the effects of optical pumping on the relative peak heights for a hyperfine spectrum of Rb. The Racah intensities are shown in red, while the intensities measured for a continuous wave (cw) laser and a pulsed laser are shown in solid black and black lines, respectively. The cw measurements deviate significantly from the Racah intensities, while the pulsed measurements are closer to the expected intensities.[1]

To illustrate the effect of mechanisms of optical pumping, consider the following: A hyperfine system has two ground states, $\mathbf{F_1}$ and $\mathbf{F_2}$, as well as an excited state $\mathbf{F_3}$, as shown in Fig. 4 When the atom is in the excited state, it has probability $P(\mathbf{F_3} \rightarrow \mathbf{F_2})$ of decaying to the $\mathbf{F_2}$ state, and probability $1 - P(\mathbf{F_3} \rightarrow \mathbf{F_2})$ of decaying to the $\mathbf{F_1}$ state. If the atom is exposed to a laser resonant with the $\mathbf{F_2} \rightarrow \mathbf{F_3}$ transition, what is the probability that after time t the ground state of the atom is still $\mathbf{F_2}$? Say that the lifetime of the $\mathbf{F_2} \rightarrow \mathbf{F_3}$ transition is τ, and that the average time for a resonant photon to

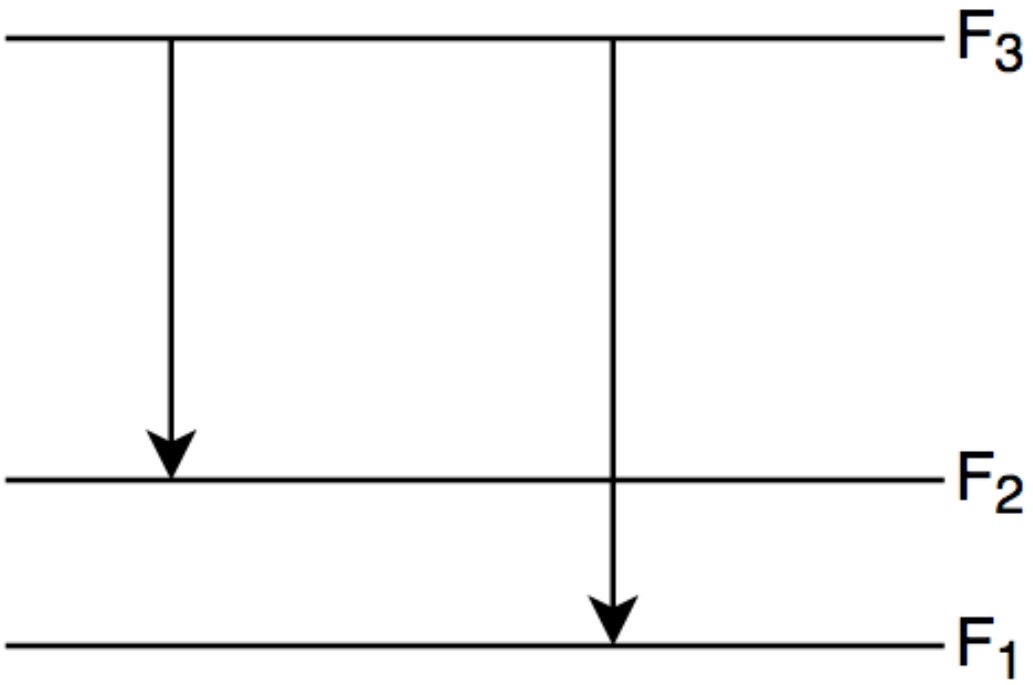

Figure 4–2: Toy model of a hyperfine system with two ground states, $\mathbf{F_1}$ and $\mathbf{F_2}$, and a single excited state $\mathbf{F_3}$. If this system is exposed to a laser resonant with the $\mathbf{F_2} \rightarrow \mathbf{F_3}$ transition, then as the atom goes through excitation and decay cycles, the chances of having an electron in $\mathbf{F_2}$ available for excitation decrease.

be absorbed is t_{abs}. Then the number of excitation/decay cycles in time t, N_{cycles}, is

$$N_{\text{cycles}} = \frac{t}{\tau + t_{\text{abs}}}. \tag{4.2}$$

rounded down to the closest integer. If at any time, the atom decays to the $\mathbf{F_1}$ state, then it is no longer on resonance and the chances of a photon being absorbed are negligible. As such, the probability that the atom is in $\mathbf{F_2}$ after N_{cycles} is

$$P(\mathbf{F_2}) = \mathbf{P}(\mathbf{F_3} \rightarrow \mathbf{F_2})^{\mathbf{N}_{\text{cycles}}} \tag{4.3}$$

As $P(\mathbf{F_3} \rightarrow \mathbf{F_2}) < \mathbf{1}$, then the chances of finding an electron in the $\mathbf{F_2}$ state decrease as t increases. If, for example, one began measuring the number of resonant photons emitted after time t for a collection of atoms with the above

hyperfine structure, the number of photons measured would be reduced by a factor of $P(\mathbf{F_2})$. This calculation is the basis for the method used in this work to measure the effect of optical pumping on the atoms being investigated at the CFBS, presented in the following section.

4.1 Optical Pumping as a Modification to the Racah Intensities

To evaluate the effects of optical pumping on a hyperfine spectrum collected at the CFBS experiment, the toy model presented above need only be expanded on. The important quantities are the time an atom interacts with the laser before entering the LCR, the time it takes for a resonant photon to be absorbed, the lifetimes of each excited state and the probability of an electron decaying to the ground state from which it originated. The computation of each of these quantities is presented in this section, after which they are combined to show how the Racah intensity for each transition must be modified to show the effects of optical pumping.

4.1.1 Interaction Time

The interaction time, t_{int} is the time that the atom will be possibly be interacting with the laser before entering the LCR. It's calculation is straightforward. If the distance between the CEC and the LCR is d, and the atoms are moving at a velocity v, then the interaction time is

$$t_{\text{int}} = \frac{d}{v} \tag{4.4}$$

While d is a static quantity, v changes depending on the frequency of the laser and the resonant frequency of the transition in question. As mentioned in Chapter 2, the CFBS fixes the frequency of the laser and uses electrodes to alter the speed of the oncoming atoms, shifting the frequency observed by the atoms. Knowing the initial energy of the beam E_b and the mass of the atoms

m_a, the initial velocity of the atoms is

$$v_{\text{init}} = \sqrt{\frac{2E_b}{m_a}} \tag{4.5}$$

If the resonant frequency of a transition is f_{res} and the frequency of the laser is f_{las}, then the velocity at which the atom will observe f_{res}, v_{res}, is described by [**?**]

$$f_{\text{res}} = f_{\text{las}}\sqrt{\frac{1 + v_{\text{res}}/c}{1 - v_{\text{res}}/c}} \tag{4.6}$$

Rearranging yields the following expression for v_{res}

$$v_{\text{res}} = c\frac{(f_{\text{res}}/f_{\text{las}})^2 - 1}{(f_{\text{res}}/f_{\text{las}})^2 + 1} \tag{4.7}$$

and

$$t_{\text{int}} = \frac{d}{c}\frac{(f_{\text{res}}/f_{\text{las}})^2 + 1}{(f_{\text{res}}/f_{\text{las}})^2 - 1} \tag{4.8}$$

4.1.2 Absorption Time of a Resonant Photon

For a chosen transition, what is the expected time, t_{abs} that passes before a resonant photon is absorbed by the atom, given a laser field of intensity I? This is simply the inverse of the scattering rate, as described in Eq. 3.47, evaluated at resonance, i.e. $\delta = 0$

$$t_{\text{abs}} = \left(\frac{s_0\gamma/2}{1 + s_0}\right)^{-1} \tag{4.9}$$

4.1.3 Lifetime of an Excited State

This quantity is already know. The inverse of Eq. 3.33 gives the lifetime, τ, of a particular transition

$$\tau = \frac{3\pi\epsilon_0\hbar c^3}{\omega^3\mu^2} \tag{4.10}$$

4.1.4 Time for Excitation/Decay Cycle

Combining the results from the two above sections, the average time that it takes for an atom to go through an excitation/decay cycle, assuming that it returns to the ground state that it was in before excitation, t_{cycle}, is

$$t_{\text{cycle}} = t_{\text{abs}} + \tau \tag{4.11}$$

$$= \left(\frac{s_0\gamma/2}{1+s_0}\right)^{-1} + \frac{3\pi\epsilon_0\hbar c^3}{\omega^3\mu^2} \tag{4.12}$$

4.1.5 Probability of Returning to Original Ground State

The probability of an atom decaying to the ground state from which it was excited is computed by comparing the decay rates of all possible transitions that share the same excited state as the transition in question, i.e.,

$$P(\text{OGS}) = \frac{\gamma_{\text{OGS}}}{\sum_{\text{PT}}\gamma_{\text{PT}}} \tag{4.13}$$

where $P(\text{OGS})$ is the probability of the atom returning to the original ground state, γ_{OGS} is the decay rate of the transition that results in the return to the original ground state and γ_{PT} is the decay rate of all possible transitions that share the same excited state as the transition in question.

4.1.6 Probability of Reaching the LCR

Finally, the probability of an atom reaching the LCR without changing its ground state is given by

$$P(\text{OGS at LCR}) = \left(\frac{\gamma_{\text{OGS}}}{\sum_{\text{PT}}\gamma_{\text{PT}}}\right)^{\frac{t_{\text{int}}}{t_{\text{cycle}}}} \tag{4.14}$$

where $\frac{t_{\text{int}}}{t_{\text{cycle}}}$ is rounded down to the nearest integer, reflecting the fact the excitation/decay cycles are quantized events.

4.2 Modification of the Racah Intensities

Now that the probability of finding an atom in its original ground state when it reaches the LCR, the effects of optical pumping can be simulated through the modification of the Racah intensity for each transition. For a given transition $\mathbf{F_e} \rightarrow \mathbf{F_g}$ the modified Racah intensity, $I_{R_{\text{mod}}}$, is

$$I_{R_{\text{mod}}} = P(\mathbf{F}_g \text{ at LCR})(2F_e+1)(2F_g+1) \begin{Bmatrix} F_g & F_e & 1 \\ J_e & J_g & \text{I} \end{Bmatrix}^2 \tag{4.15}$$

$$= \left(\frac{\gamma_{\text{OGS}}}{\sum_{\text{PT}} \gamma_{\text{PT}}} \right)^{\frac{t_{\text{int}}}{t_{\text{cycle}}}} (2F_e+1)(2F_g+1) \begin{Bmatrix} F_g & F_e & 1 \\ J_e & J_g & \text{I} \end{Bmatrix}^2 \tag{4.16}$$

CHAPTER 5
Results

CHAPTER 6
Conclusion

REFERENCES

[1] Anika V. et al. The Collinear Fast Beam laser Spectroscopy experiment at TRIUMF. 2015.

[2] Carlos A. Bertulani. *Nuclear Physics in a Nutshell*. 2007.

[3] Fujia Yang, Joseph H. Hamilton. *Modern Atomic and Nuclear Physics*. 2010.

[4] G.K. Wertheim et al. Determination of the Gaussian and Lorentzian content of experimental lineshapes. *Review of Scientific Instruments*, 45, 1974.

[5] Thomas Procter. *New Techniques of Laser Spectroscopy on Exotic Isotopes of Gallium and Francium*. PhD thesis, 2013.

[6] T.J. Proctor et al. Nuclear mean-square-charge radii of $^{63,64,66,68-82}$Ga nuclei: No anomalous behavious at N = 32. 2012.